Fluvial sediment supply to a mega-delta reduced by shifting tropical-cyclone activity

Stephen E. Darby[1], Christopher R.Hackney[1], Julian Leyland[1], Matti Kummu[2], Hannu Lauri[3], Daniel R. Parsons[4] , James L. Best[5], Andrew P. Nicholas[6], Rolf Aalto[6]

[1]Geography and Environment, University of Southampton, Southampton SO17 1BJ, United Kingdom
[2]Water and Development Research Group, Aalto University, Aalto, Helsinki, Finland
[3]EIA Finland Ltd., Sinimäentie 10B, 02630 Espoo, Finland
[4]Department of Geography, Environment and Earth Sciences, University of Hull, Hull, HU6 7RX, United Kingdom
[5]Departments of Geology, Geography & GIS, Mechanical Science and Engineering and Ven Te Chow Hydrosystems Laboratory, University of Illinois, Champaign, IL 61820, USA
[6]Department of Geography, University of Exeter, Exeter, EX4 4RJ, United Kingdom

The world's rivers deliver 19 billion tonnes of sediment to the coastal zone annually[1], with a significant fraction being sequestered in large deltas, home to over 500 million people. Most (>70%) large deltas are under threat from a combination of rising sea levels, ground surface subsidence and anthropogenic sediment trapping[2,3], and a sustainable supply of fluvial sediment is therefore critical in preventing deltas being 'drowned' by rising relative sea levels[2,3,4]. Here, we combine suspended sediment load data from the Mekong River with hydrological model simulations to isolate the role of tropical cyclones (TCs) in transmitting suspended sediment to one of the world's great deltas. We demonstrate that spatial variations in the Mekong's suspended sediment load are correlated (r = 0.765, p < 0.1) with observed variations in TC climatology, and that a significant portion (32%) of the suspended sediment load reaching the delta is delivered by runoff generated by TC-associated rainfall. Furthermore, we estimate that the suspended load to the delta has declined by 52.6 ± 10.2 Mt over recent years (1981-2005), of which 33.0 ± 7.1 Mt is due to a shift in TC climatology. Consequently TCs play a significant role in controlling the magnitude of, and variability in, transmission of suspended sediment to the coast. It is likely that

anthropogenic sediment trapping in upstream reservoirs is a dominant factor in explaining past[5,6,7,8], and anticipating future[9,10], declines in suspended sediment loads reaching the world's major deltas. However, our study shows that changes in TC climatology affect trends in fluvial suspended sediment loads and thus are key to fully assessing the risk posed to vulnerable coastal systems.

The world's largest rivers contribute a disproportionately large fraction (Extended Data Table 1) of the terrestrial sediment flux, which has both created, and is critical in sustaining, their great deltas. Moreover, river borne sediments are a key vector for carbon and nutrients, thereby playing a vital role in global biogeochemical cycles[11,12]. However, a significant majority (>70%) of large deltas are now recognized as being under severe threat from rising relative sea levels[2,3], in part due to reported anthropogenically-driven reductions in sediment loads[5,6,7,8]. Many large rivers are located in tropical regions (Extended Data Figure 1) that exhibit highly seasonal flow regimes affected by tropical cyclones (TCs). Previous work has shown that TCs can deliver much higher than normal levels of rainfall, effectively triggering landslides and mobilizing sediments into the river network, thereby generating very high instantaneous sediment loads[13,14,15], showing that TCs are effective agents of erosion in uplands. However, notwithstanding some prior studies in smaller drainage basins[16,17], the role of TCs in driving sediment delivery to the lowlands and coast remains unclear. As noted, this is particularly the case for large rivers that carry much of the terrestrial sediment flux because these rivers are, in their mid- to lower- reaches, typically bound by massive floodplains that can sequester significant volumes of suspended sediment into storage during floods[18]. Here we address this uncertainty by quantifying the significance of TCs in driving suspended sediment loads through an exemplar mega-river, the Mekong.

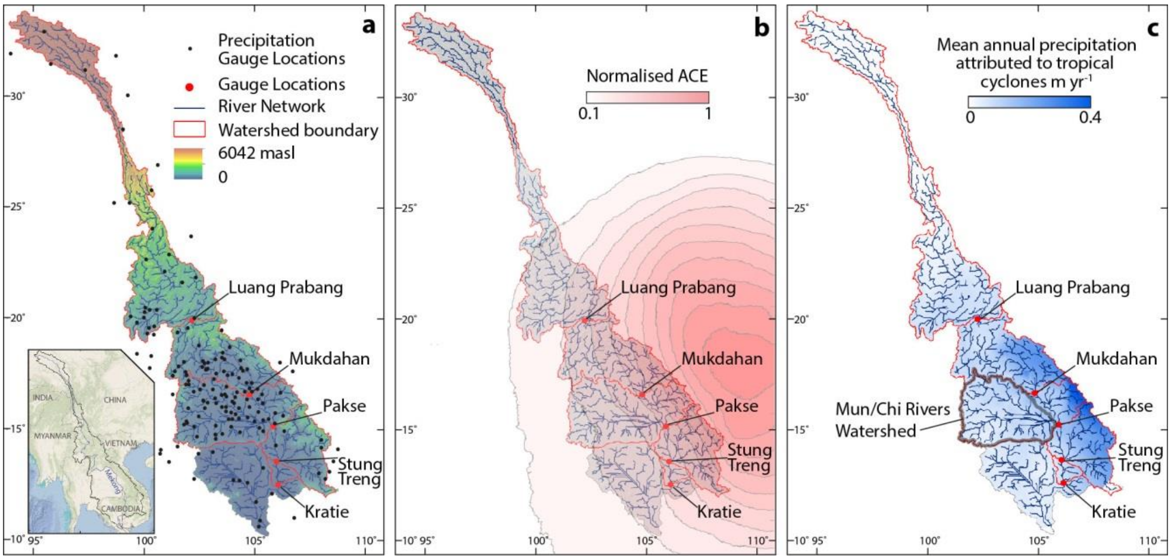

Figure 1. The hydrometereological gauging network of the Mekong River and associated tropical cyclone climatology. **a**, Locations of hydrological stations at Luang Prabang (19.892765º N 102.133603º E; upstream drainage area, A = 323,600 km^2), Mukdahan (16.542981º N 104.731914º E, A = 464,100 km^2), Pakse (15.113891º N 105.801083º E, A = 632,600 km^2), Stung Treng (13.524850º N 105.942341º E, A = 722,300 km^2) and Kratie (12.481499º N 106.017898º E, A = 734,200 km^2) in the Mekong River drainage basin, also showing the topography of the basin and the locations of the meteorological stations used herein. **b**, Climatology of tropical cyclones as represented by a normalized Accumulated Cyclone Energy (ACE)[42] metric during 1981-2005. **c,** Estimates of mean annual rainfall associated with tropical cyclones during 1981-2005. Details of the procedures used to estimate the rainfall associated with tropical cyclones and the ACE metric are given in the Methods.

Draining the Tibetan Plateau and the Annamite Mountains bordering Laos and Vietnam (**Fig. 1**), and with the monsoonal climate generating intense rainfall, the Mekong basin (795,000 km^2) generates fluxes of water (450 km^3 yr^{-1})[19] and sediment (~160 Mt yr^{-1}, but see below)[20] that rank tenth and ninth, respectively, amongst the world's great rivers[1]. The Mekong is therefore similar to other major rivers (e.g., Ganges-Brahmaputra, Yangtze, Mississippi) that transmit globally significant sediment loads and that are influenced in their mid to lower courses by TCs. Similar to these other rivers, the sediments of the Mekong River have resulted in the formation of a large delta, with significant contemporary debate on the extent to which declining sediment loads may in the future increase the vulnerability of the Mekong delta to rising sea-level[7,9,21].

To quantify the influence of TCs on the suspended sediment transport regime, we determined temporal (25 years) and spatial (1400 km study reach) variations in suspended solids loads throughout the Lower Mekong River (see Methods). Specifically, we first employed a distributed hydrological model, forced with two climate scenarios, one with and the other without observed TCs, to simulate water discharges at five river gauging stations (see Methods for model details and **Fig. 1** for gauging station locations): Luang Prabang in Laos (LP), Mukdahan in Thailand (MK), Pakse in Laos (PX), and Stung Treng (ST) and Kratie (KT), both in Cambodia. Importantly, these five river gauging stations are situated on an environmental gradient that spans regions that are weakly (LP) to moderately (MK, PX) to strongly (ST, KT) affected by TCs (**Figs 1b**, **1c**). We then analysed archival measurements of suspended solids concentration, collected by the respective national hydrological agencies, to construct new suspended sediment rating curves - statistical functions linking the rate of suspended sediment transport to water discharge - for the five stations (see Methods and Extended Data Figure 2). These rating curves were then used with the model-simulated water discharges to compute suspended solids loads and to apportion these loads into TC-driven components (Q_{s_TC}) using:

$$Q_{s\_TC} = Q_s \left(\frac{Q_{sim\_TC}}{Q_{sim}}\right) \qquad (1)$$

where Q_s is the total suspended sediment load as computed using the sediment rating curves with the total simulated flow discharge, Q_{sim} (*i.e.*, the flow discharge for the baseline scenario with the observed climatology including TCs), and Q_{sim_TC} is the proportion of the simulated flow discharge attributable to TCs. The quantity Q_{sim_TC} in Eq. (1) is determined by differencing the flow discharges computed in the two scenarios with (Q_{sim}) and without (Q_{no_TC}) TCs, such that $Q_{sim\_TC} = Q_{sim} - Q_{no\_TC}$.

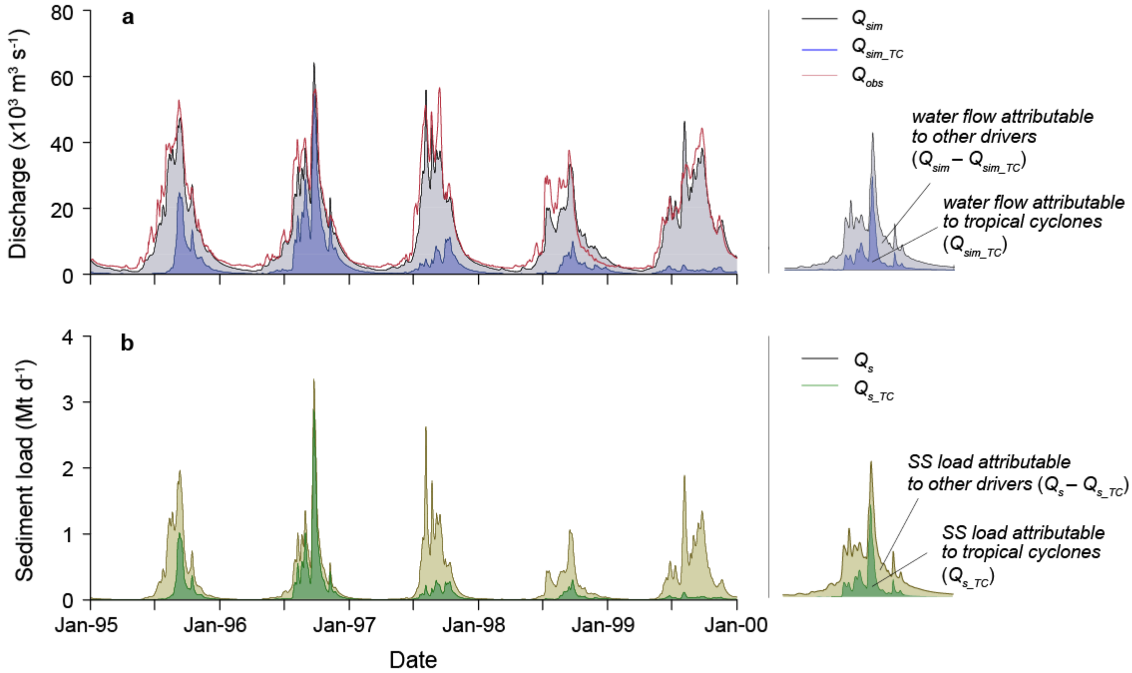

Figure 2. Daily flow discharge and suspended solids load at Kratie during 1st January 1995 to 31st December 1999. **a**, Daily simulated (Q_{sim}) and observed (Q_{obs}) water flows, along with the daily water flows attributable to tropical cyclones (Q_{sim_TC}). **b,** Daily total suspended solids load (Q_s; in megatonnes per day) and daily suspended solids load attributable to tropical cyclones (Q_{s_TC}; also in megatonnes per day). Note that the period 1995 to 1999 encompasses the years during the 1981-2005 study period that are the most (1996) and least (1999) strongly affected by tropical cyclones.

The hydrological model predicts water discharges that closely match historical records (as an example we show data for Kratie in **Fig. 2a**, but results for all other stations are shown in Extended Data Figure 3, with fit statistics summarized in Extended Data Table 2). Notable peaks and troughs in the total simulated flow discharge (Q_{sim}) and the flow discharge attributable to TCs (Q_{sim_TC}) are evident. These variable flows force significant fluctuations in simulated instantaneous suspended sediment loads, but notably there are multiple TC-forced suspended sediment transport events in most years (as indicated by the peaks in **Fig. 2b**). Integrating over the 25-year study period then yields estimates of mean annual suspended sediment load (Extended Data Table 3). Our estimate for Kratie (87.4 ± 28.7 Mt yr^{-1}), the station closest to the apex of the Mekong delta, falls within the lower limit of the range (~81 Mt yr^{-1} to 111 Mt yr^{-1}) of recent estimates[1,22,23], although it is substantially less than the *c*. 150 – 170 Mt yr^{-1} cited by older studies[19,24] based on less reliable datasets.

Importantly, our results illustrate the extent to which the modest (at annual timescales) rainfall totals associated with TCs nevertheless effectively generate runoff and suspended sediment transport. During 1981-2005, TCs only delivered between 1.8% (above Luang Prabang) and 4.7% (above Kratie) of annual rainfall, but generated between 13.7% (Luang Prabang) and 28.8% (Kratie) of annual runoff. The proportion of the mean annual suspended sediment load forced by TC-associated runoff is greater still, varying between 15.2% (Luang Prabang) and 31.7% (Kratie) (Extended Data Table 3). There are two reasons for this amplification effect. First, TC-derived rainfall is strongly seasonal, falling largely during, or just after, the monsoon months, when catchments are pre-wetted; consequently TC-associated rainfall is very effective in generating runoff[25]. Second, the sediment rating functions linking suspended sediment flux and water discharge possess exponents with values exceeding unity (Extended Data Figure 3), meaning that the peak flows generated by TCs promote very high instantaneous suspended sediment fluxes. Therefore, suspended sediment transport associated with TCs contributes substantially to mean annual loads, with the former correlating well (r = 0.765, p = 0.099) with the time-averaged TC climatology as represented by the 1981-2005 Accumulated Cyclone Energy (ACE; Extended Data Table 3).

Temporal trends in annual suspended sediment load (Q_s), and the component of that load associated with TCs (Q_{s_TC}), during 1981-2005 are shown for Kratie in **Fig. 3** (results for all the other stations are shown in Extended Data Figure 4). Nonparametric Mann-Kendall tests (see Methods) reveal that there have been declines in both Q_s and Q_{s_TC} at three (Mukdahan, Stung Treng, and Kratie) of the four stations that are either moderately or strongly influenced by TCs (the exception is Pakse, as discussed below). As expected, the station that is only weakly affected by TCs (Luang Prabang, Extended Data Fig. 4a) does not exhibit any significant trends in Q_s or Q_{s_TC} that are not artefacts of the response of this station to upstream damming. Importantly, recent historical declines in Q_s at Mukdahan, Stung Treng and Kratie (Extended Data Figure 4 and **Fig. 3**) are driven to a large extent by declines in the suspended sediment load attributable to TCs (Q_{s_TC}). Specifically, at Mukdahan 62% of the 21.4 Mt decline in Q_s between 1981 and 2005 is attributable to reducing Q_{s_TC} (Extended Data Fig. 4b). At the Cambodian stations, 44% (Stung Treng; Extended Data Fig. 4d) and 61% (Kratie; **Fig. 3**) of the declines in Q_s are attributable to reducing Q_{s_TC}. Thus, the response of Q_s over time is intimately tied to the extent to which upstream catchments receive TC-derived rainfall (Extended Data Figure 5).

As noted above, Pakse is exceptional in that it is moderately influenced by TCs (4.1% of annual rainfall is associated with TCs), but TC-driven runoff (8.4%) and suspended sediment loads (9.3%) are both anomalously low compared to Mukdahan, Stung Treng and Kratie (Extended Data Table 2). However, TC-associated rainfall is less hydrologically effective at Pakse because flows there are strongly influenced by inflows from a major west bank tributary system, the Mun/Chi, that joins immediately upstream of the gauge and which drains a region that is only mildly influenced by TCs (**Fig. 1**). Additionally, the exponent in the suspended sediment rating curve at Pakse is much less than those at Stung Treng and Kratie (Extended Data Figure 2), meaning the higher flows associated with TCs generate comparatively lower instantaneous suspended sediment transport rates.

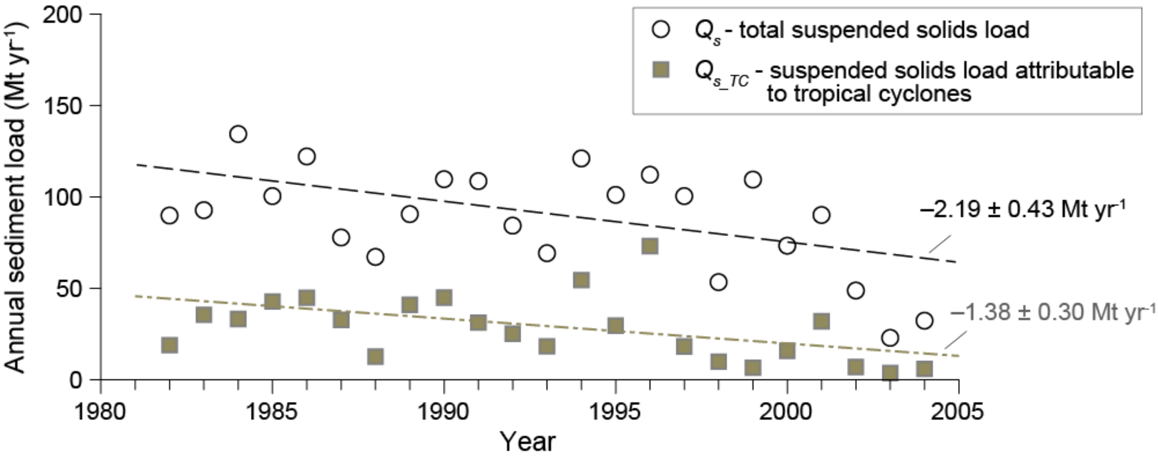

Figure 3. Time series of annual suspended solids loads at Kratie during 1982 to 2004. The total annual suspended solids load (Q_s; megatonnes per year) and suspended solids load attributable to tropical cyclones (Q_{s_TC}; also in megatonnes per year) are shown with significant ($p < 0.05$) trends as identified by Mann-Kendall analysis indicated by the dashed lines. The numerical value of the time-rate of change of annual suspended solids load (with error) is also indicated for each of the trend lines.

Our results are the first to demonstrate the substantial extent to which tropical cyclones are effective in transmitting suspended sediment load through the lowlands of large rivers, a finding that has profound implications. A substantial portion (~40 to 50%)[26] of the suspended sediment load of the Mekong River is deposited in its delta, home to 20 million people and the rice basket of SE Asia[21,27]. Significant concerns have been raised regarding the scale of recent and projected future reductions in the sediment load reaching the delta, as a result of sand mining[21,28] and upstream damming[9,10,21]. However, our study reveals that during the period 1981-2005, the Mekong at Kratie is estimated to have experienced a cumulative loss of 33.0 ± 7.1 Mt of its suspended sediment load (**Fig. 3**) as a result of changes in precipitation delivered by TCs crossing the Mekong basin (Extended Data Figure 5). Limitations in the observational data make it challenging to fully contextualize the 1981-2005 trends in TC climatology, that are the focus of this paper, within the longer term historical record (Extended Data Figure 6). Nevertheless, our key finding, namely that changes in TC climatology represent a significant, but previously neglected, driver of suspended sediment transmission through the Mekong River, remains robust. Furthermore, high-resolution climate models indicate that although the number and intensity of TCs tracking across the South China Sea will likely increase under future anthropogenic climate change, their track locations will shift eastwards and away from the Indochina peninsula, leading to net reductions in ACE over the Mekong basin[29]. If these projected reductions in ACE are correct, TC-driven suspended sediment delivery to the Mekong delta will decline still further, exacerbating projected declines in sediment loads due to damming[8,9,10] and sand mining and placing the delta at even greater risk. Although our data focus on the suspended sediment load, the delivery of bedload sediment, which is important in the construction, or restoration, of deltas[30], would also be lessened by a reduction in cyclone-associated sedimentation. Furthermore, other large rivers that transport a significant proportion of the global sediment flux are also affected by TCs. Our study indicates that their deltas may also be much more significantly affected by, and vulnerable to, changes in tropical cyclone climatology than assumed in current assessments of the impacts of future environmental change.

References

1. Milliman, J. D. and Farnsworth, K. L. *River discharge to the coastal ocean: A global synthesis*, Cambridge University Press, Cambridge (2011).
2. Ericson, J. P., Vörösmarty, C. J., Dingman, S. L., Ward, L. G., Meybeck, M. Effective sea-level rise and deltas: Causes of change and human dimension implications. *Glob. Plan. Change*. **50**, 63-82; doi: 10.1016/j.globplacha.2005.07.004 (2006).
3. Syvitski, J. P. M *et al*. Sinking deltas due to human activities. *Nat. Geosci*. **2**, 681-686 (2009).
4. Darby, S. E., Dunn, F. E., Nicholls, R. J., Rahman, M. and Riddy, L. P. A first look at the influence of anthropogenic climate change on the future delivery of fluvial sediment to the Ganges–Brahmaputra–Meghna delta. *Environ.Sci: Processes Impacts* **17**, 1587-1600; doi: 10.1039/C5EM00252D (2015).

5. Vörösmarty, C. J. *et al*. Anthropogenic sediment retention: major global impact from registered river impoundments. *Glob. Planet. Change* **39**, 169-190; doi:10.1016/S0921-8181(03)00023-7 (2003).
6. Walling, D. E. and Fang, D. Recent trends in the suspended sediment loads of the world's rivers. *Glob. Plan. Change* **39**, 111-126 (2003).
7. Giosan, L., Syvitski, J. P. M., Constatinescu, S. and Day, J. Protect the world's deltas. *Nature* **516**, 31-33 (2014).
8. Shuai Wang *et al*. Reduced sediment transport in the Yellow River due to anthropogenic changes. *Nat. Geosci*. **9**, 38-42; doi: 10.1038/NGEO2602 (2016).
9. Kummu, M. J., Wang, J. J., Lu, X. X. and Varis, O. Basin-wide sediment trapping efficiency of emerging reservoirs along the Mekong. *Geomorphology* **119**, 181-197; doi:10.1016/j.geomorph.2010.03.018 (2010).
10. Kondolf, G. M., Rubin, Z. K. and Minear, J. T. Dams on the Mekong: Cumulative sediment starvation. *Water Resour. Res*. **50**, 5158–5169; doi:10.1002/2013WR014651 (2014).
11. Richey, J. E., Brock, J. T., Naiman, R. J., Wissmar, R. C. and Stallard, R. F. Organic Carbon: Oxidation and transport in the Amazon River. *Science* **207**, 1348-1351 (1980).
12. Aufdenkampe, A. K. et al. Riverine coupling of biogeochemical cycles between land, oceans, and atmosphere. *Frontiers in Ecology and Environment* **9**, 53-60; doi:10.1890/100014 (2011).
13. Milliman, J. D. and Kao, S. J. Hyperpycnal discharge of fluvial sediment to the ocean: Impact of Super-Typhoon Herb (1996) on Taiwanese rivers. *J. Geol*. **113**, 503-516 (1996).
14. Dadson, S. J. *et al*. Links between erosion, runoff variability and seismicity in the Taiwan orogen. *Nature* **426**, 648-651; doi: 10.1038/nature02150 (2003).
15. Hilton, R. G. *et al*. Tropical-cyclone driven erosion of the terrestrial biosphere from mountains. *Nat. Geosci*. **1**, 759-762 (2008).
16. Terry, J. P., Garimella, S. and Kostaschuk, R. A. Rates of floodplain accretion in a tropical island river system impacted by cyclones and large floods. *Geomorphology* **42**, 171-182; doi:10.1016/S0169-555X(01)00084-8 (2002).
17. Amos, K. J., *et al*. Supply limited sediment transport in a high-discharge event of the tropical Burdekin River, North Queensland, Australia. *Sedimentology* **51**, 145-162 (2004).
18. Aalto, R. *et al*. Episodic sediment accumulation on Amazonian floodplains influenced by El Niño/Southern Oscillation. *Nature* **425,** 493-497; doi:10.1038/nature02002 (2003).
19. Mekong River Commission (MRC). *Overview of the Hydrology of the Mekong River Basin, Mekong River Commission*. Vientiane, Laos (2005).
20. Milliman, J. D. and Meade, R. H. World-wide delivery of river sediment to the oceans. *J. Geol*. **91**, 1-21 (1983).

21. Anthony, E. J., *et al*. Linking rapid erosion of the Mekong River delta to human activities. *Sci. Rep*. **5**, 1475; doi: 10.1038/srep1475 (2015).
22. Kummu, M. and Varis, O. Sediment-related impacts due to upstream reservoir trapping on the Lower Mekong River. *Geomorphology* **85**, 275-293; doi: 10.1016/j.geomorph.2006.03.024 (2007).
23. Lu, X. X., Kummu, M. and Oeurng, C. Reappraisal of sediment dynamics in the Lower Mekong River, Cambodia. *Earth Surf. Proc. Landforms* **39**, 1855-1865; doi:10.1002/esp.3573 (2014).
24. Wang, J. J., Lu, X. X. and Kummu, M. Sediment load estimates and variations in the lower Mekong River. *River Res. & Applications* **27**, 33-46 (2011).
25. Darby, S.E. *et al*. Decoding the drivers of bank erosion on the Mekong River: The roles of the Asian monsoon, tropical storms, and snowmelt. *Wat. Resour. Res*. **49**, 2146-2163; doi: 10.1002/wrcr.20205 (2013).
26. Manh, N. V., Dung, N. V., Hung, N. N., Merz, B. and Apel, H. Large-scale suspended sediment transport and sediment deposition in the Mekong delta. *Hydrol. Earth Syst. Sci*., **18**, 3033-3053; doi: 10.5194/hess-18-3033-2014 (2014).
27. Kontgis, C., Schneider, A. and Ozdogan, M. Mapping rice paddy extent and intensification in the Vietnamese Mekong River Delta with dense time stacks of Landsat data. *Remote Sens. Env*. **169**, 255-269; doi: 10.1016/j.rse.2015.08.004 (2015).
28. Brunier, G., Anthony, E. J., Goichot, M., Provansal, M. and Dussouillez, P. Recent morphological changes in the Mekong and Bassac river channels, Mekong Delta: The marked impact of river-bed mining and implications for delta destabilisation. *Geomorphology* **224**, 177-191; doi:10.1016/j.geomorph.2014.07.009 (2014).
29. Redmond, G., Hodges, K. I., Mcsweeney, C., Jones, R. and Hein, D. Projected changes in tropical cyclones over Vietnam and the South China Sea using a 25 km regional climate model perturbed physics ensemble. *Clim. Dyn*. **45**, 1983-2000; doi: 10.1007/s00382-014-2450-8 (2014).
30. Nittrouer, J. A. and Viparelli, E. Sand as a stable and sustainable resource for nourishing the Mississippi River delta. *Nat. Geosci*. **7**, 350-354; doi: 10.1038/ngeo2142 (2014).

Supplementary Information is available.

Acknowledgements

This study was supported by awards NE/JO21970/1, NE/JO21571/1 and NE/JO21881/1 from the UK Natural Environmental Research Council (NERC) and the Academy of Finland funded project SCART (grant number 267463). We thank the Mekong River Commission for access to hydrological and suspended sediment data and the Department for Hydrology and Water Resources in Cambodia for aDcp data and their logistical support. J.L.B was also in receipt of a University of Southampton Diamond Jubilee Fellowship and National Great Rivers Research and Education Centre Fellowship that aided completion of this work.

Author Contributions

S.E.D., J.L., C.H., D.P., J.L.B., A.P.N. and R.A. jointly conceived the study. C.H., S.E.D., J.L., J.L.B and D.P. collected and processed the field data. C.H. constructed the sediment rating curves and, with S.E.D., undertook the data analysis. M.K. and H.L. conducted the model simulations, with the tropical cyclone track data and rainfall anomalies being computed by J.L. S.E.D. drafted the paper, which was then edited by all co-authors.

Author information

The authors declare no competing financial interests. Correspondence and requests for materials should be addressed to S.E.D. (S.E.Darby@soton.ac.uk).

Methods

Hydrological Model. The VMod hydrological model[31] was selected based on its success in prior studies of the Mekong River basin[25,32,33]. As implemented for the Mekong River, VMod employs a 5×5 km (25 km^2) grid, with surface elevation, gradient, aspect, vegetation and soil type in each cell being extracted from the SRTM DEM[34], GLC2000 land cover[35] and FAO soil-type[36] data sets, respectively.

VMod simulations were forced using daily rainfall and temperature data estimated from a network of 151 meteorological stations (**Fig. 1a**). Specifically, the precipitation data employed herein are from the Mekong River Commission (MRC) hydrometeorological database[37], supplemented with GSOD (Global Surface Summary of the Day) data[38] for the Chinese part of the basin. These data have been carefully quality controlled[32], and the MRC data therefore represent the highest quality available data, with the best density of precipitation stations. However, as is frequently the case in developing nations, resource constraints have meant that there has not yet been a more recent release of the MRC product, constraining our study to the period 1981-2005. However, also pertinent to this choice of study period is the fact that in 2005 the total active storage of all dams on the Mekong was 7.2 km^3, of which the active storage of Chinese dams was only 0.8 km^3, meaning that the potential impact of dams is still rather minor at this date[9]. In contrast, by the year 2015 these figures had increased to ~55 km^3 and 24 km^3, respectively.

Estimates of daily rainfall totals and temperatures within each VMod grid cell were obtained by interpolating from the three nearest observations using inverse distance squared weighting. For daily rainfall totals, a multiplicative elevation correction (with coefficient 0.0002 mm m^{-1}) was employed to account for differences of elevation between each observation point and the location of the grid cell, whereas the temperature data were corrected for elevation using a lapse rate of −0.006 K m^{-1}. VMod simulates snowmelt using a degree-day model, in which the amount of snowmelt is obtained from daily average temperature exceeding a given threshold multiplied by a snowmelt coefficient K_{melt}. The model also computes snow evaporation, snowpack water storage, and refreezing. The snowmelt parameters employed herein were calibrated in a previous study[32] using flow measurements at the Chiang Saeng gauging station. Glacier melt is computed similarly to snowmelt, albeit using a different set of parameters and the assumption of infinite storage.

In VMod the flow discharge is routed along a river network that is generated using DEM and map data. Each model grid cell has a river, either starting at that grid cell or flowing through it, to which the runoff from the cell is added. Flow within the river network is computed using a 1-dimensional river model with a kinematic wave approximation. In this way simulated runoff at any point in the network reflects both the local and upstream contributions of precipitation, with the precipitation being deconstructed into cyclone and non-cyclone components as described in the *Rainfall Scenarios* section, below. Note that, in the flow routing process, river cross-sections are represented using two superimposed trapezoids, with the lower one representing the main channel and the upper the floodplain, allowing for a representation of the effects of overbank storage on downstream attenuation of the flood wave.

Fig. 2 (for Kratie, along with the left hand panels of Extended Data Figure 3 for the other hydrological stations) shows a comparison of simulated VMod versus observed runoff regimes at each of the gauging stations employed in this study. Note that, for clarity, **Fig. 2** shows data only for the period 1995–2000, a period that includes the years that are most and least affected by TCs, but the goodness of fit measures reported here are for the entire simulation period (1 May 1981 to 31 March 2005). The four goodness of fit measures used are: (i) the mean discrepancy ratio for daily flows (*Me*), which is the average of all the ratios (computed at each daily time step) of simulated to observed daily water flows, with $Me = 1$ indicating perfect agreement between simulated and observed data; (ii) the mean discrepancy ratio for annual peak flows (Me_p); (iii) the root mean square error (*RMSE*), and; (iv) the Nash-Sutcliffe Index (NSI)[37]. Based on these metrics (Extended Data Table 2) VMod, on average, under-predicts daily water flows throughout the study reach, while under-predicting the annual flood maxima in the lower parts (Stung Treng and Kratie) and over-predicting annual flood maxima in the upper parts (Luang Prabang, Mukdahan and Pakse) of the reach (**Fig. 2**, Extended Data Figure 3 and Extended Data Table 2). Nevertheless, with NSI values varying between 0.749 (Luang Prabang) and 0.922 (Pakse), the overall performance VMod of is either "Very Good" (Luang Prabang, Mukdahan, Stung Treng) or "Excellent" (Pakse, Kratie), based on the classification scheme of Henriksen *et al*.[40]

Rainfall Scenarios and Tropical Cyclone Climatology. The hydrological model as described above was run with two rainfall scenarios. The first "baseline" scenario replicated actual conditions in the 1981-2005 study period and employed observed rainfall totals. In the second scenario, these baseline totals were revised downwards by removing the rainfall estimated to have been delivered by tropical cyclones. The simulated runoff associated with tropical cyclones (Q_{sim_TC}) was then computed by differencing the daily flows simulated under the two scenarios.

To estimate rainfall totals associated with tropical cyclones, we first employed the IBTrACS (version v03r02) storm tracks database[41] to locate the paths, at daily time steps, of all recorded tropical cyclones intersecting or passing near the Mekong Basin during 1981–2005. Rainfall anomalies associated with these storm paths were then defined by first interpolating, using the nearest neighbour, daily rainfall values observed at the network of 151 stations used in the baseline rainfall scenario onto a 0.1° (~11 km^2)

resolution grid. Next, all rainfall stations located within a 500 km Haversine search radius[42,43] from the centroid of the storm on that date were identified. These identified stations were then temporarily (for the specific time step) removed from the analysis and an updated rainfall surface (minus the identified stations) was re-interpolated onto the same 0.1° grid. A rainfall anomaly surface, representing estimated rainfall associated with the identified storm and time step, was obtained by differencing the original and updated surfaces. This process was repeated for each daily time step, allowing the observed rainfall series at each meteorological station to be adjusted by subtracting rainfall anomalies within the grid square specific to each gauge from the observed daily rainfall totals. Note that since the hydrometeorological database we used in this analysis does not discriminate between precipitation associated or not associated with tropical cyclones, it is not possible to validate our estimates of cyclone-derived precipitation. For this reason, our estimates of rainfall associated with tropical cyclones are deliberately based on a method (nearest neighbour interpolation) that is more conservative than prior studies[43] that simply assume that *all* rainfall within the assigned search radius is related to tropical cyclones. By the same token, while acknowledging that there is uncertainty regarding the typical radii of tropical cyclones, our decision to employ a 500 km search radius is again conservative in that it is at the lower end of the range of values typically employed in prior studies[44].

The IBTrACS data on which the above analyses are founded comprise six hourly best-track positions and intensity estimates. Only storms designated as in a tropical phase with one-minute maximum sustained surface wind speeds exceeding 34-knots (17.5 ms^{-1}) are included in our analysis. The IBTrACS data were also used to compute the accumulated cyclone energy (ACE) metric[45] that we employ to characterize the TC climatology over the Mekong River basin for the period 1981-2005. The ACE parameter is analogous to the power dissipation index (PDI)[46] in that it convolves intensity and duration information for each individual TC observed in a defined area (here the sub-basins for the five gauging stations that are the focus of this study), offering considerable advantages over definitions based on the more familiar categorizations based on wind speed[47]. In this context, our estimates of ACE are obtained by squaring the 6-hourly intensity estimates reported in the best-track database and integrating over the 1981-2005 study period.

Sediment Rating Curves. Sediment rating curves of the form:

$$C = a\,Q^{b} \tag{1}$$

were constructed for each hydrological station on the Mekong River mainstem below the China-Laos border and upstream of the Mekong delta by fitting observed suspended solids concentration (SSC; *C*) and observed water discharge (*Q*) data (Extended Data Table 4) using non-linear estimation techniques constructed using the Curve Fitting Toolbox in Matlab version R2014a. Specifically, a non-linear least squares power law solver with one term was applied to the raw data, using the Trust-Region algorithm. The use of the power law solver follows previous work[48,49,50] in optimizing the fit at the higher values of discharge and concentration that dominate overall transport. This procedure results in a poor fit for low discharges at Pakse (Extended Data Figure 2) but using an alternative solver, designed to improve the low fit, is not justified. This is because doing so makes only a very minor (< 2%) difference in the mean annual sediment load at Pakse while introducing significant errors into the more important high-flow fits at the other stations. Note that our focus on suspended, rather than total, sediment load is not problematic since bed load is less than 20% of the total load (based on comparisons of rivers from the data compilation of Turowski *et al*.[51] with suspended sediment concentrations similar to those of the Mekong River).

In terms of the data sources feeding into the sediment rating curves (Extended Data Table 4), at Luang Prabang, Mukdahan and Pakse the SSC and water discharge data were obtained from hydrological records archived by the Mekong River Commission (MRC; available to download from http://portal.mrcmekong.org/index). However, the MRC SSC measurements are available only sporadically and have been acquired using a range of methodologies (reflecting the different approaches taken by differing hydrological agencies in this trans-national river) at the different gauging stations (Extended Data Table 4). All of the MRC's SSC measurements at Mukdahan were collected using USGS designed isokinetic depth-integrated samplers (USGS D49 samplers) deployed at three verticals over the cross-section. The three samples are composited to provide a single sample from which the suspended sediment concentration (SSC) is determined[49]. For the stations in Laos (i.e., Luang Prabang and Pakse), the MRC SSC data were initially (1961) collected for a brief period using the same procedures as at Mukdahan, but subsequently the depth-integrated samplers were replaced with USGS P61 point-integrating samplers. To avoid potential problems with mixed sampling protocols in the datasets, and because depth-integrated sampling relies heavily on the even ascent of the sampler through the water column, to avoid biasing the SSC we excluded the relatively few data obtained using depth-integrated samplers from further consideration. The point-integrated samplers were deployed at three verticals over the cross-section, at heights of 0.2, 0.5 and 0.8 of the flow depth in the case of the point-sample (producing nine individual samples, from which the mean SSC for the cross-section is obtained by simple averaging). However, as shown in Extended Data Figure 7, because the concentration of suspended sediment varies, both through the water column and laterally over the cross-section, simple averaging of point-based samples systematically biases the resulting estimate of the cross-section averaged SSC (relative to that obtained from alternative quasi-synoptic sampling techniques). We corrected for this effect by reducing the SSC values recorded within the MRC database by 26% for all the Laos and Thai stations (Extended Data Figure 7). We derived this correction factor by comparing the averaged cross-section SSC computed from acoustic Doppler current profiler (aDcp) surveys in Cambodia, these aDcp surveys being undertaken as part of an aDcp field calibration exercise designed to retrieve SSC data from aDcp records archived by the Cambodian hydrological agency.

For the stations at Stung Treng and Kratie, sediment rating curves were constructed using flow discharge and SSC data (Extended Data Table 4) retrieved from the archives of the Cambodian Department of Hydrology and Water Resources (DHRW). These DHRW data were acquired via deployments of a four-beam 600 kHz aDcp (RD Instruments) during routine surveys undertaken in the period 2009 to 2014 by DHRW personnel. These aDcp surveys do not directly record suspended solids concentrations, but rather the archived DHRW data files contain acoustic backscatter (ABS) information recorded during the original surveys. We retrieved suspended solids concentrations from these ABS data by means of a calibration function (Extended Data Figure 7) that we derived based on 54 point measurements of SSC deployed contemporaneously with the DHRW aDcp to record coeval ABS values in the same parcel of water following past guidelines[52,53,54]. In this field calibration procedure, the SSC data were obtained by filtering (Whatman GF/C glass microfiber grade 47mm diameter 1.2 μm filter paper) and weighing the mass of solids retained from water samples collected at a wide range of flow depths and channel locations using a 3-litre Van Dorn sampler[55] during fieldwork that was spread over a wide range of flow conditions during 2013 and 2014. Consequently, the calibration function encompasses a wide range of SSC and ABS data. Analysis of ABS values and the suspended sediment grain size collected from the point samples reveals there is no relationship between the two, likely due of the narrow range of grain sizes within the LMR[56]. Since the aDcp data provide a quasi-synoptic (less a blanking zone of 0.5 m at the top of the water column and a side-lobe interference zone of 10% of the flow depth at the bottom of the water column) image of ABS over the channel cross-section, the calibration function can be used to transform the ABS data to an accurate estimate of section-averaged SSC (Extended Data Figure 7), as also noted above.

Having derived the rating curves for each gauging station (Extended Data Figure 2), we then explicitly investigated whether the rating curves exhibit hysteresis effects associated with sediment exhaustion, which might be expected to lead to lower SSC values for a given discharge on the falling versus rising stages of the annual flood wave. However, no such evidence of hysteresis was identified (see Extended Data Figure 2), presumably due to fluctuations in SSC being subdued due to the large catchment areas and consequent effects of channel and floodplain storage in attenuating the peaks[24].

We also considered whether there is a shift in sediment transport during flows affected by TCs, for example as a result of increased sediment supply from catchment erosion during storms. Specifically, we evaluated whether there are differences in sediment rating curves for flows that are (using the VMod model outputs to identify TC-affected flows and then cross-matching to identify SSC measurements that are TC affected) or are not affected by TCs. As indicated in Extended Data Table 4, this enabled us to identify 34 SSC samples during TC affected flows at Luang Prabang (14% of all observations at that station), whilst 30 samples were identified during TC affected flows at Mukdahan (3% of observations). We found there were no significant (ANOVA, $p > 0.05$) differences between sediment ratings developed using the TC-affected versus the non-TC affected SSC data at either station. This indicates that we can with confidence apply single rating curves for these stations, for both TC-affected and TC-unaffected flows. Since we are only able to discriminate TC-affected flows from VMod outputs during the 1981-2005 study period, and because there are no SSC data from this period at Stung Treng and Kratie, and there are too few SSC data at Pakse to identify any TC-affected measurements, there are no data to complete a similar formal analysis at these other three stations (Extended Data Table 4). Nevertheless, the very tight fit of these three stations' ratings (Extended Data Figure 2), alongside the point that these stations are TC-affected during the period of SSC data collection, indicates that any shift in sediment transport processes during TCs is unlikely to have any material effects on the estimation of suspended solid loads at these locations.

Bearing in mind the relatively long periods over which the SSC data used to construct the sediment ratings at Luang Prabang, Mukdahan and Pakse were collected (Extended Data Table 4), we also tested for the possibility that varying ENSO phase, a known cause of hydroclimatological variability in the Mekong River, may lead to non-stationarity in the SSC values at these stations[57,58], using dummy variable regression analysis. Letting Z = 1 if ENSO phase is positive (i.e., El Niño) and 0 otherwise, then for the slope of the regression:

$$y = \beta_0 + \beta_1 ZX + \beta_2 X + \varepsilon \tag{2}$$

$$y = \begin{cases} \beta_0 + (\beta_1 + \beta_2)X + \varepsilon & if\ ENSO\ phase\ is\ positive \\ \beta_0 + \beta_2 X + \varepsilon & if\ ENSO\ phase\ is\ negative \end{cases} \tag{3}$$

Then, for the intercept of the regression:

$$y = \beta_0 + \beta_1 Z + \beta_2 X + \varepsilon \tag{4}$$

$$y = \begin{cases} (\beta_0 + \beta_1) + X + \varepsilon & if\ ENSO\ phase\ is\ positive \\ \beta_0 + X + \varepsilon & if\ ENSO\ phase\ is\ negative \end{cases} \quad (5)$$

Or, for both slope and intercept:

$$y = \beta_0 + \beta_1 Z + \beta_2 X + \beta_3 + \varepsilon \quad (6)$$

$$y = \begin{cases} (\beta_0 + \beta_1) + (\beta_2 + \beta_3)X + \varepsilon & if\ ENSO\ phase\ is\ positive \\ \beta_0 + \beta_3 X + \varepsilon & if\ ENSO\ phase\ is\ negative \end{cases} \quad (7)$$

We found no significant difference at the 0.05 significance level (ANOVA on dummy variable regression coefficients for each site) in the SSCs, for a given *Q*, as a function of ENSO phase, demonstrating that there is therefore no evident bias in the SSCs introduced as a function of climate variability associated with ENSO. With the completion of the first significant main-stem cascade of dams on the Chinese portion of the Mekong River in 1993, we also considered whether the SSC data differ pre- and post- 1993. Accordingly, a similar analysis (Eqs 2 – 7) was conducted for those sites (Luang Prabang and Mukdahan) at which SSC samples span the pre- and post- dam periods. We found that at Mukdahan no significant difference exists at the 0.05 significance level (ANOVA on dummy variable regression coefficients), implying there is no reason to split the data based on the pre- and post- dam periods. However, a significant difference ($p < 0.05$) between the pre- and post- dam periods does exist at Luang Prabang (ANOVA test statistic = 9.7377, n = 236, df = 1, 232). Consequently, at Luang Prabang, we calculate suspended solids loads (see below) using the pre- and post- dam rating curves (Extended Data Figure 2) for the periods 1981-1992 and 1993-2005, respectively. Finally, we emphasize that our analysis does not account for anthropogenic factors, such as flow regulation through reservoirs, land-use or land cover change, or increasing sediment mining, that could potentially introduce a trend into the relationships between flow discharge and suspended sediment concentration at each gauging station. Our suspended sediment rating curves therefore assume stationarity of these factors over the 1981-2005 study period.

Sediment Load Estimation. The lack of hysteresis and apparent stationarity of the SSC data means that we were able to employ a single (two at Luang Prabang, one for the pre- and one for the post- dam periods) sediment rating curve specific to each station (Extended Data Figure 2), together with the continuous water discharge records obtained from our hydrological modelling, to estimate daily suspended solids loads (**Fig. 2**; Extended Data Figure 3) for the 1981-2005 study period. These daily loads were in turn used to compute, by summation, the annual sediment loads for each station (**Fig. 3**; Extended Data Figure 4). Note that since the modelling period extended from 1st May 1981 to 31st March 2005, we report annual sediment loads only for those years (1982 to 2004 inclusive) for which full-year records are available. Mean annual suspended solids loads for each station over the 22-year period (1982 to 2004) were then obtained by calculating the arithmetic mean of these annual loads (Extended Data Table 3).

Statistical Analysis. Mann-Kendall[59] tests, used to evaluate whether there are significant (at 95% confidence) temporal trends (the magnitude of the trend being equated to Sen's slope, with uncertainty equated to the 95% confidence bounds on the Sen slope estimates) in the computed annual sediment loads, were computed in Matlab R2014a using the ktaub.m file written by Jeff Burkey (2006), which is available from the Matlab Exchange at http://www.mathworks.com/matlabcentral/fileexchange/11190-mann-kendall-tau-b-with-sen-s-method--enhanced-/content/ktaub.m

Data: The precipitation and temperature data used in the hydrological model simulations are taken from the Mekong River Commission (MRC) hydrometeorological database[37] (not available online) supplemented with GSOD (Global Surface Summary of the Day) data[38] for the Chinese part of the basin (ftp://ftp.ncdc.noaa.gov/pub/data/gsod/ years 1981-2005). The IBTrACS (version v03r02) storm tracks database[41] that we used estimate the track locations and hence precipitation anomalies associated with tropical cyclones was downloaded from the IBTrACS website (https://www.ncdc.noaa.gov/ibtracs/index.php?name=ibtracs-data IBTrACS-All data v03r02 all storms line shapefile). Note that we are not able to make the input data files used in the hydrological model simulations available as the precipitation and temperature data are from the MRC (as described above) under a licence which precludes redistribution of products or derived products. Water discharge data used in the validation of the hydrological model are from the hydrological records archived in the MRC data portal (http://portal.mrcmekong.org/index as discharge records from Luang Prabang (station ID 011201 unique dataset ID 21301), Mukdahan (station ID 013402 unique dataset ID 3301), Pakse (station ID 013901 unique dataset ID 3141), Stung Treng (station ID 014501 unique dataset ID 2809), and Kratie (station ID 014901 unique dataset ID 2811)), as are the suspended sediment concentration data (available from http://portal.mrcmekong.org/index as sediment concentration records from station ID 011201 unique dataset ID 4746, station ID 013402 unique dataset ID 4849, and station ID 013901 unique dataset ID, 4773, respectively) used to derive the sediment rating curves at Luang Prabang, Mukdahan, Pakse. The aDcp data files used to derive the sediment rating curves for the stations at Stung Treng and Kratie are available on request from the Cambodian Department of Hydrology and River Works (DHRW; http://www.dhrw-cam.org/index.php).

Code Sharing: The VMod hydrological model software as employed in this study is available to download from www.eia.fi/vmod.The related analytical code comprises the bespoke Matlab scripts, authored by Dr Julian Leyland, that were used to partition out the cyclone-influenced rainfall as described in the text. These scripts are not publically available as they are currently being developed and used in commercial applications.

References

31. Koponen, J.H. *et al*. *HBV and IWRM Watershed Modelling User Guide*, MRC Information and Knowledge Management Programme. Available at http://www.eia.fi/index.php/support/download (2010).
32. Lauri, H. et al. Future changes in Mekong River hydrology: impact of climate change and reservoir operation on discharge. *Hydrol. Earth Sys. Sci*. **16**, 4603-4619; doi: 10.5194/hess-16-4603-2012 (2012).
33. Lauri, H. VMod 5km *Grid Hydrological Modeling Report (EIA Ltd.)*. Aalto University, Finland (2009).
34. Jarvis, A., H. *et al*. Hole-Filled Seamless SRTM Data V4, Int. Cent. for Trop. Agric. (CIAT) Available at http://srtm.csi.cgiar.org (2008).
35. IES. *Global Land Cover 2000* Available at http://ies.jrc.ec.europa.eu/global-land-cover-2000 (2000).
36. FAO. *WRB Map of World Soil Resources*. Available at http://www.fao.org/ag/agl/agll/wrb/soilres.stm. (2003).
37. Mekong River Commission. *Hydrometeorological database of the Mekong River Commission*. Mekong River Commission (MRC), Vientiane, Lao PDR (2011).
38. NCDC. *Global Surface Summary of the Day (GSOD)*, US National Climatic Data Center (NCDC) Data available at ftp://ftp.ncdc.noaa.gov/pub/data/gsod (2010).
39. Nash, J.E. & Sutcliffe, J.V. River flow forecasting through conceptual models part I—A discussion of principles. *J. Hydrol.* **10**, 282–290 (1970).
40. Henriksen, H. J. *et al*. Assessment of exploitable groundwater resources of Denmark by use of ensemble resource indicators and a numerical groundwater–surface water model. *J. Hydrol.* **348**, 224–240 (2008).
41. Knapp, KR. *et al*. The international best track archive for climate stewardship (IBTrACS): Unifying tropical cyclone best track data. *Bull. Am. Meterol. Soc.* **91**, 363–376 (2010).

42. Rodgers, E.B. *et al*. Contribution of tropical cyclones to the North Pacific climatological rainfall as observed from satellites. *J. Appl. Meteorol.* **39**, 1658–1678 (2000).
43. Englehart, P.J. & Douglas, A.V. The role of eastern North Pacific tropical storms in the rainfall climatology of western Mexico. *Int. J. Climatol.* **21**, 1357–1370 (2001).
44. Kubota, H. & Wang, B. How much do tropical cyclones affect seasonal and inter-annual rainfall variability over the Western North Pacific? *J. Climate* **22**, 5495–5510 (2009).
45. Bell, G.D., et al. Climate assessment for 1999. *Bull. Am. Meteorol. Soc.* **81**, s1–s50; doi:10.1175/1520-0477(2000)81[s1:CAF]2.0.CO;2. (2000).
46. Emanuel, K. Increasing destructiveness of tropical cyclones over the past 30 years. *Nature* **436**, 686-688; doi:10.1038/nature03906 (2005).
47. Webster, P.J. *et al*. Changes in tropical cyclone number, duration and intensity in a warming environment. *Science* **309**, 1844-1846; doi:10.1126/science.1116448 (2005).
48. Ferguson, R.I. River loads underestimated by rating curves. *Wat. Resour. Res*. **22**, 74-76 (1986).
49. Walling, D.E. *Evaluation and analysis of sediment data from the Lower Mekong River*. Mekong River Commission, Vientiane, Laos (2005).
50. Walling, D.E. The changing sediment load of the Mekong River. *Ambio* **37**, 150-157 (2008).
51. Turowski, J.M., Rickenmann, D. and Dadson, S.J. The partitioning of the total sediment load of a river into suspended load and bedload: a review of empirical data. *Sedimentology* **57**, 1126–1146; doi: 10.1111/j.1365-3091.2009.01140.x (2010).
52. Kostachuk, R.J. *et al.* Measurement of flow velocity and sediment transport with an acoustic Doppler current profiler. *Geomorphology* **68**, 25 – 37 (2005).
53. Szupiany, R.N. *et al.* Morphology, flow structure and suspended bed sediment transport at two large braid-bar confluences. *Wat. Resour. Res.* **45**, W05415; doi:10.1029/2008WR007428 (2009).
54. Shugar, D. *et al.* On the relationship between flow and suspended sediment transport over the crest of a sand dune, Rio Parana, Argentina. *Sedimentology* **57**, 252-272 (2010).
55. Van Dorn, W.G. Large-volume water samplers. *Eos Trans. AGU* **37**, 682–684; doi:10.1029/TR037i006p00682 (1956).
56. Bravard, J-P., Goichot, M. and Tronchère, H. An assessment of sediment-transport processes in the Lower Mekong River based on deposit grain sizes, the CM technique and flow-energy data. *Geomorphology* **207**, 174-189 (2014).
57. Räsänen, T. & Kummu, M. Spatiotemporal influences of ENSO on precipitation and flood pulse in the Mekong River Basin. *J. Hydrology* **476**, 154 – 168 (2013).
58. Ward, P.J. *et al.* Annual flood sensitivity to El Niño Southern Oscillation at the global scale. *Hydrol. Earth Syst. Sci.* **18**, 47-66 (2013).
59. Kendall, M. G. A new measure of rank correlation. *Biometrika* **30**, 81–93 (1938).

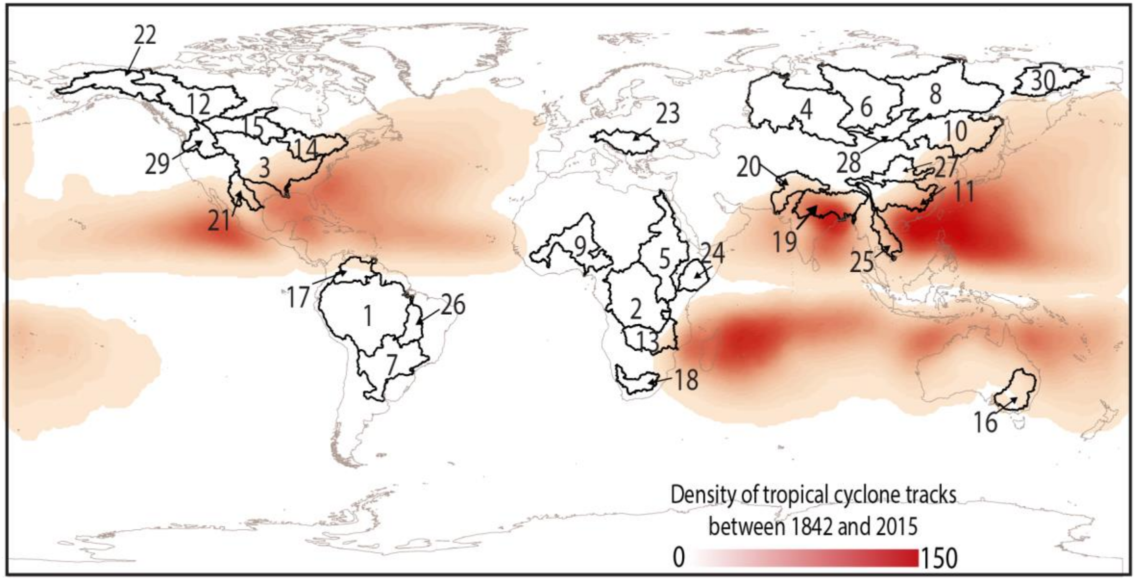

Extended Data Figure 1

Extended Data Table 1.

Basin ID	Basin Name	Drainage Area (10^6 km^2)	Mean annual runoff (km^3 yr^{-1})	Mean annual sediment flux (Mt yr^{-1})
1	Amazon	6.3	6300	1200
2	Congo	3.8	1300	43
3	Mississippi	3.3	490	120
4	Ob	3.0	390	16
5	Nile	2.9	30	0.2
6	Yenisei	2.6	620	4.1
7	Parana	2.6	530	90
8	Lena	2.5	520	20
9	Niger	2.2	160	40
10	Amur	1.9	350	52
11	Yangtze	1.8	900	470
12	Mackenzie	1.8	310	100
13	Zambezi	1.3	100	9
14	St. Lawrence	1.2	340	4.6
15	Nelson	1.1	89	n/a
16	Murray-Darling	1.1	7.9	1
17	Orinoco	1.1	1100	210
18	Orange	1.0	4.5	17
19	Ganges	0.98	490	520
20	Indus	0.98	5	10
21	Rio Grande	0.87	0.7	0.7
22	Yukon	0.85	210	54
23	Danube	0.82	210	42
24	Shebelle	0.81	19	n/a
25	Mekong	0.80	450	110
26	Tocantins	0.76	370	75
27	Yellow	0.75	15	150
28	Brahmaputra	0.67	630	540
29	Columbia	0.67	240	9.7
30	Kolyma	0.60	120	10

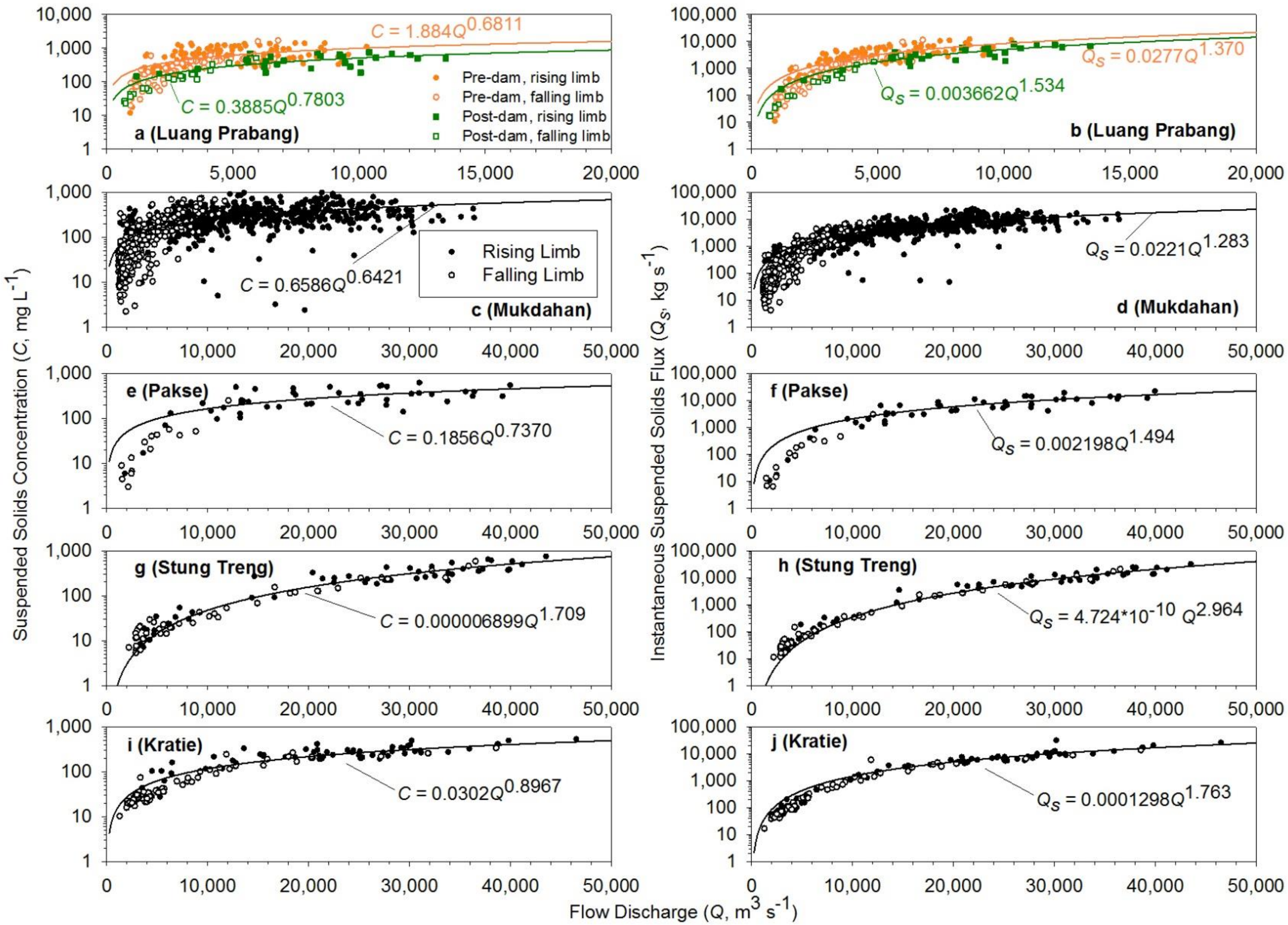

684

685 **Extended Data Figure 2**

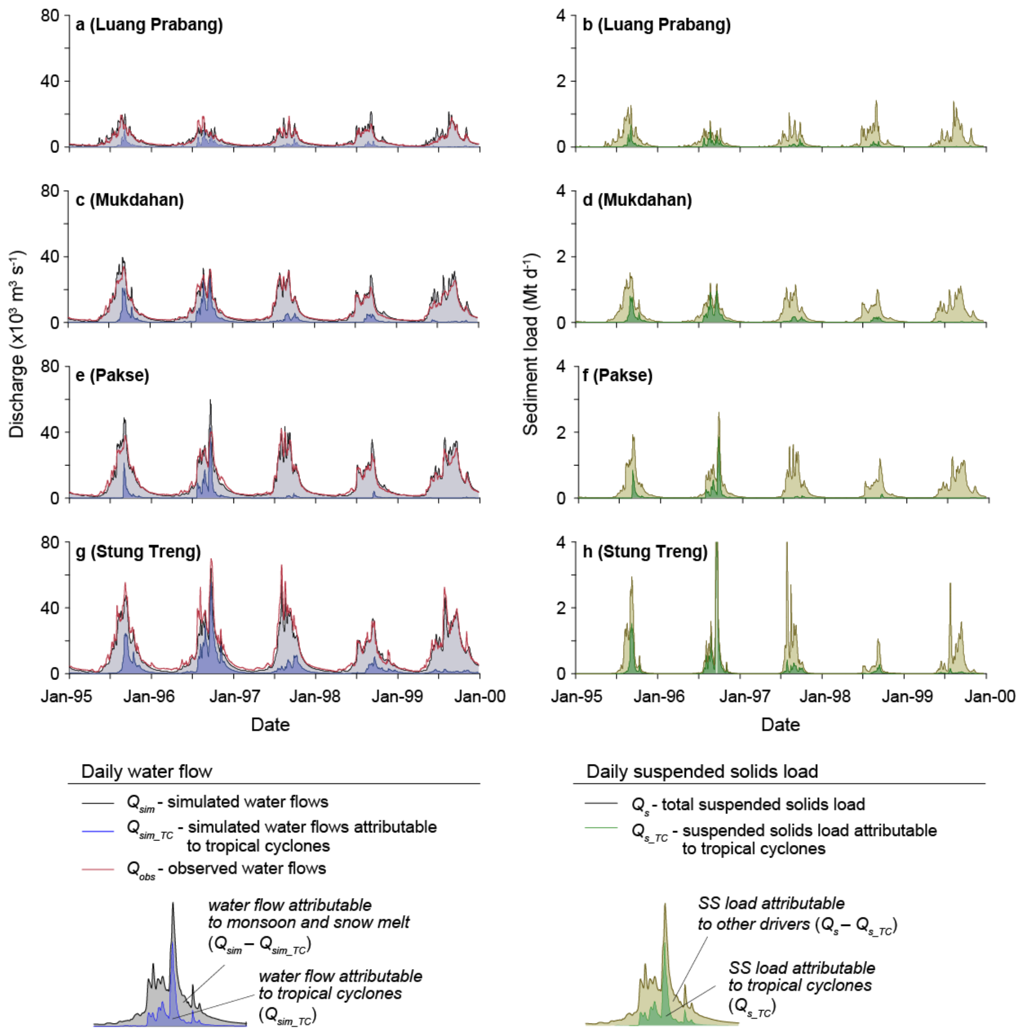

Extended Data Figure 3.

Extended Data Table 2.

River Gauging Station	Goodness of Fit Measures			
	Mean Discrepancy Ratio – Daily Flows (Me)	Mean Discrepancy Ratio - Annual Peaks (Me_p)	Root Mean Square Error ($RMSE$, $m^3 s^{-1}$)	Nash-Sutcliffe Index (NSI)
Luang Prabang	0.99	1.19	1690	0.749
Mukdahan	0.87	1.08	3170	0.821
Pakse	0.89	1.15	2700	0.922
Stung Treng	0.73	0.84	6210	0.789
Kratie	0.77	0.89	5800	0.808

Extended Data Table 3.

River Gauging Station	**Accumulated Cyclone Energy** (ACE, 10^4 kn^2)	**Rainfall** (P, mm)	**Rainfall due to Tropical Cyclones** ($P_{\_TC}$, mm)	**Runoff** (Q, m^3 yr^{-1})	**Runoff due to Tropical Cyclones** ($Q_{\_TC}$, m^3 yr^{-1})	**Suspended Solids Load** (Q_s, Mt yr^{-1})	**Suspended Solids Load due to Tropical Cyclones** (Q_{s_TC}, Mt yr^{-1})	**Proportion of Load Forced by Tropical Cyclones** (%)
Luang Prabang	0.12	1157	21	3945	540	70.4 ± 21.8	10.7 ± 6.4	15.2
Mukdahan	2.84	1346	47	7230	1550	73.4 ± 15.9	16.5 ± 9.3	22.5
Pakse	3.49	1356	56	9155	770	79.8 ± 19.0	7.5 ± 6.6	9.3
Stung Treng	5.64	1436	67	10375	2960	71.3 ± 36.3	24.2 ± 19.3	34.0
Kratie	5.76	1438	67	10490	3020	87.4 ± 28.7	27.7 ± 17.6	31.7

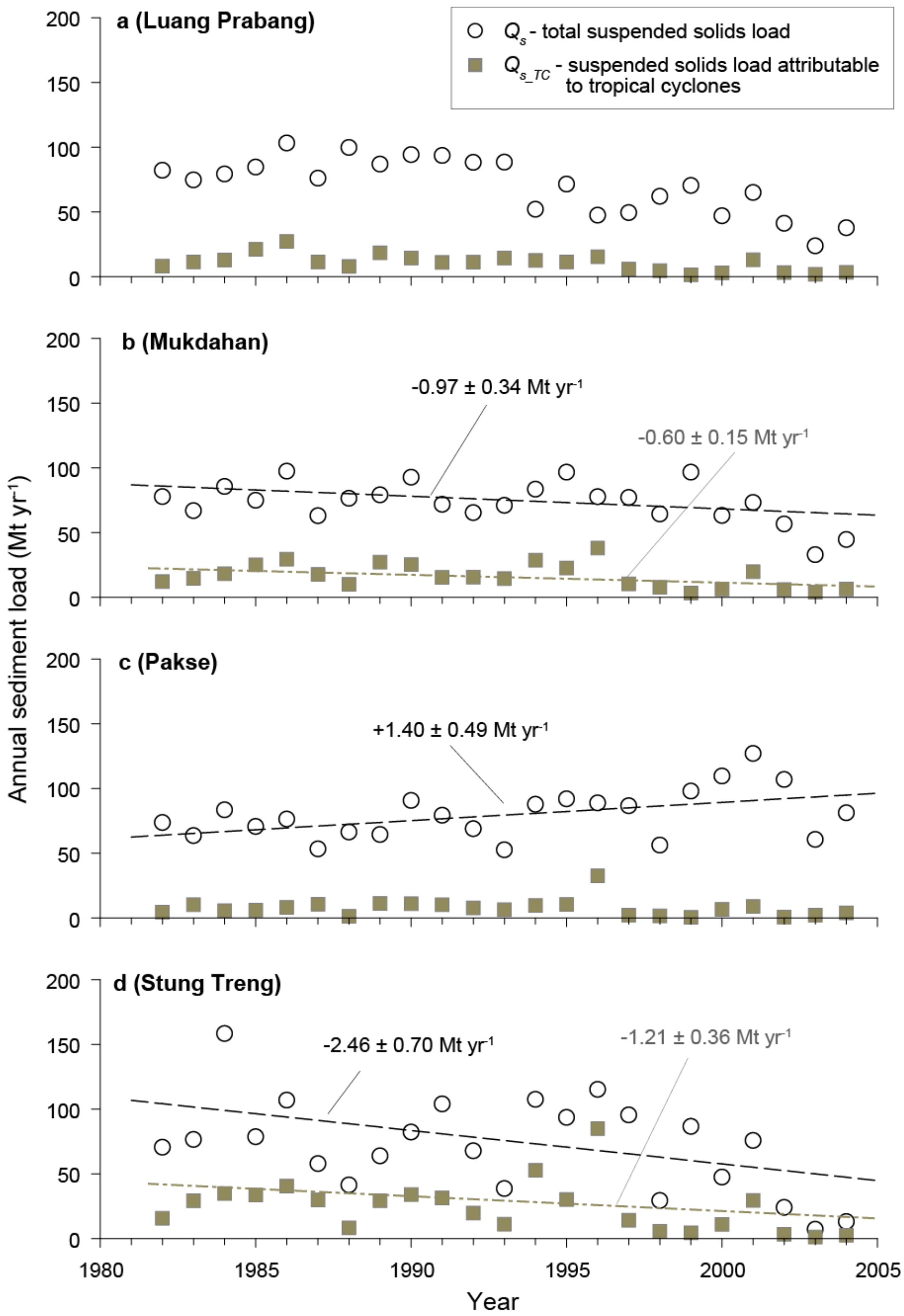

695

696 **Extended Data Figure 4**

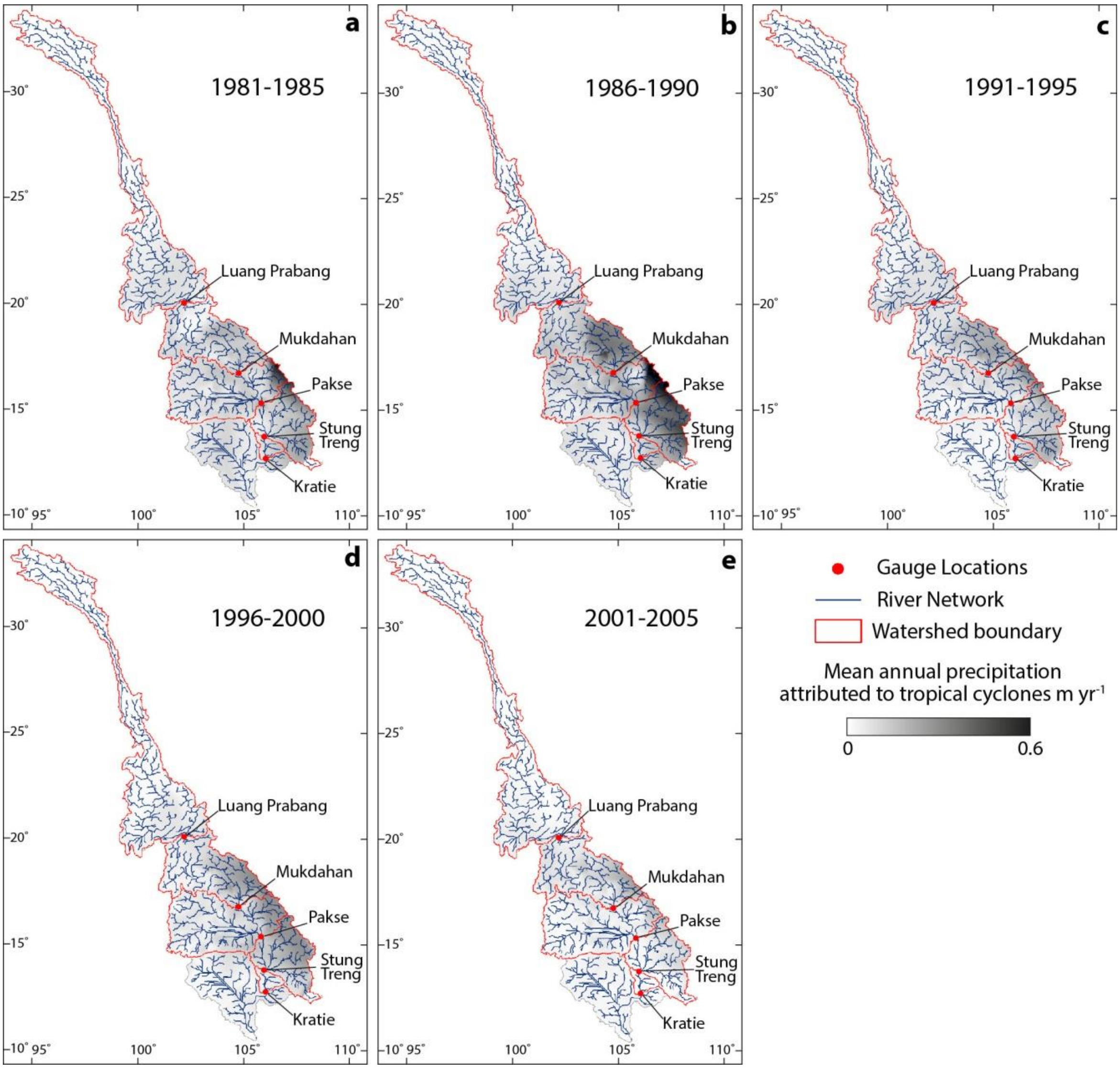

Extended Data Figure 5.

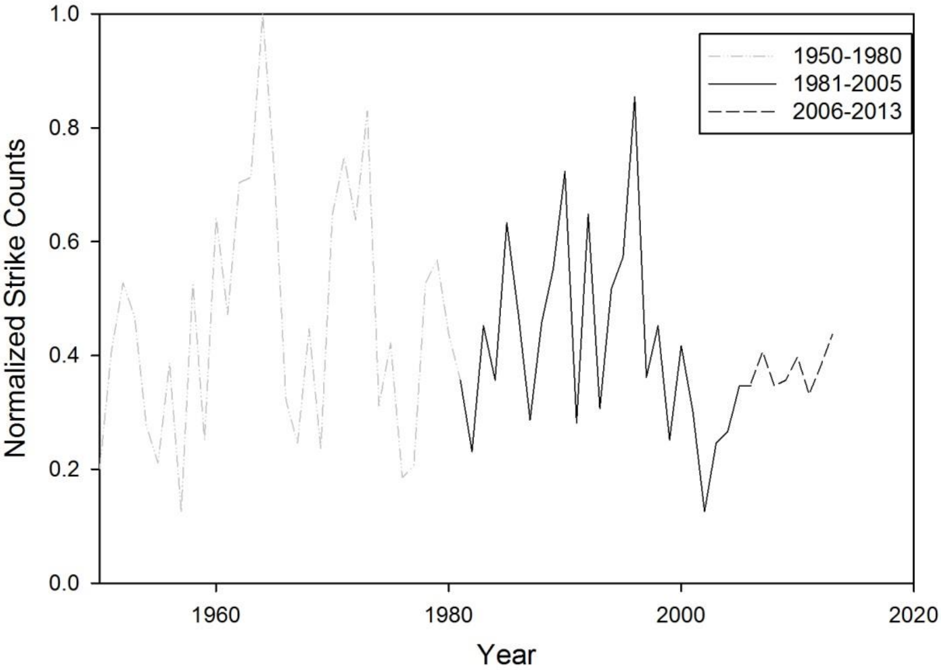

Extended Data Figure 6.

Extended Data Table 4.

Gauging Station	Number of Samples	Period of Data Availability	Sampling Method
Luang Prabang	236 (34)	1986-1989; 1992; 1997-2000; 2002	Point-integrated
Mukdahan	1159 (30)	1962-1965; 1967-1980; 1982; 1991-1994; 1996-1997; 1999-2007	Depth-integrated
Pakse	60 (0)	1998-2002	Point-integrated
Stung Treng	95 (0)	2009-2014	aDcp backscatter
Kratie	140 (0)	2009-2014	aDcp backscatter

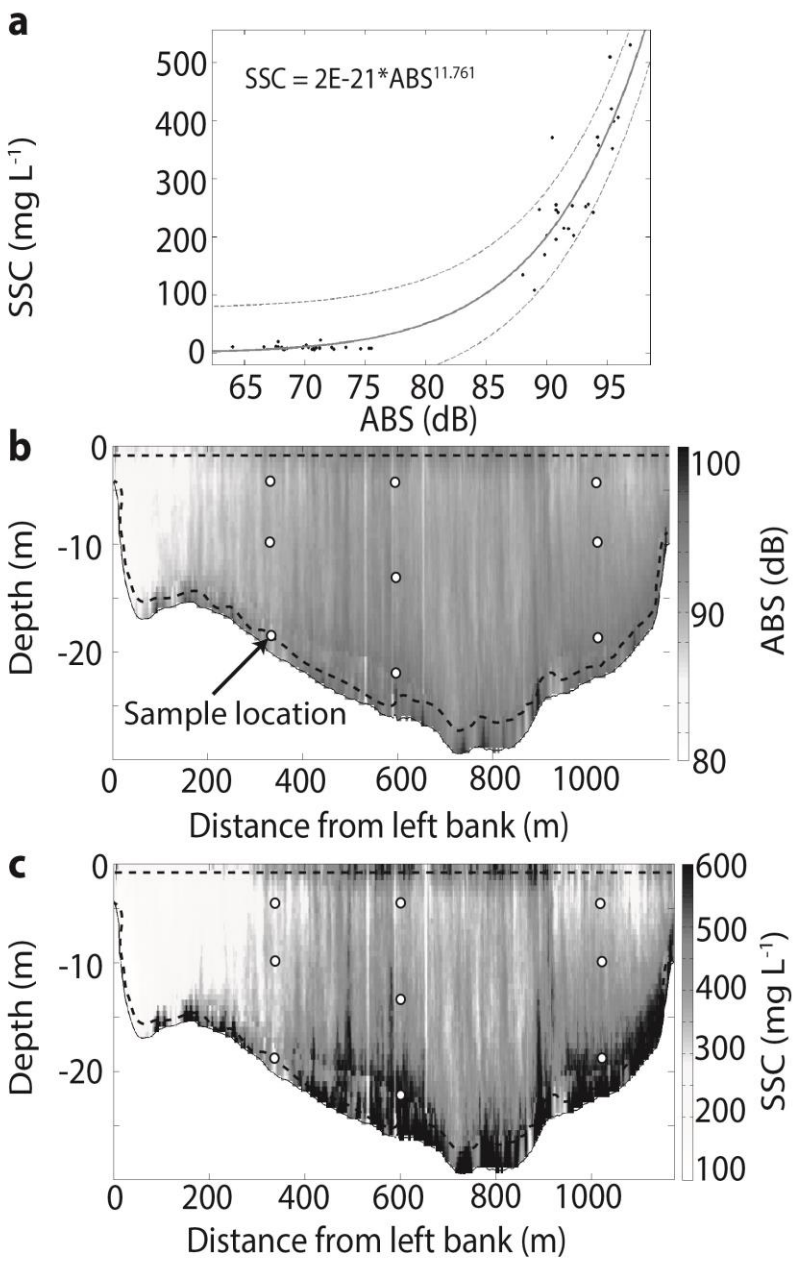

712
713 **Extended Data Figure 7.**
714

Extended Data Figure and Table Captions

Extended Data Table 1. Overview of the drainage area, mean annual runoff and mean annual sediment yield for the world's 30 largest rivers as defined by drainage area, with data from Milliman and Farnsworth (2011)[1]. The ID numbers identify the locations of the drainage basins shown on Extended Data Figure 1. The data indicate that the sediment loads from these 30 largest rivers together sum to 3.92 billion tonnes per year, a significant proportion (20.6%) of the total global riverine flux as estimated by Milliman and Farnsworth (2011).

Extended Data Figure 1. Locations of the world's 30 largest (by drainage area) rivers (the numbers identify the basins listed in Extended Data Table 1) in relation to the density of all tropical cyclone tracks from 1842 to 2015 as recorded in the IBTrACS[41] database. Track density was calculated using the point density function in ArcGIS 10.1.

Extended Data Figure 2. Sediment rating curves for the five river gauging stations on the Lower Mekong River. The left hand panels show the relationship between flow discharge (Q) and suspended solids concentration (C) at: **a,** Luang Prabang (pre-dam: n = 187, r^2 = 0.338; post-dam: n = 49, r^2 = 0.648); **c,** Mukdahan (n = 1159, r^2 = 0.497); **e,** Pakse (n = 60, r^2 = 0.591); **g,** Stung Treng (n = 95, r^2 = 0.870), and; **i,** Kratie (n = 140, r^2 = 0.850). The right hand panels show how the relationships on the left-hand panels propagate through to give the relationship between flow discharge (Q) and instantaneous sediment load (Q_s) at the same stations: **b,** Luang Prabang (pre-dam: n = 187, r^2 = 0.791; post-dam: n = 49, r^2 = 0.864); **d,** Mukdahan (n = 1159, r^2 = 0.693); **f,** Pakse (n = 60, r^2 = 0.780); **h,** Stung Treng (n = 95, r^2 = 0.900), and; **j,** Kratie (n = 140, r^2 = 0.931). All the fits shown are significant at $p < 0.00001$. Note that the scales for subplots **a** and **b** (Luang Prabang) differ from those for the other subplots. We recognize that the fits for Q versus Q_s on the right hand panels are stronger than the fits between Q and C because of the auto-correlation arising when transforming C to Q_s ($Q_s = C \times Q/1000$). For the stations at Mukdahan, Pakse, Stung Treng and Kratie, a single rating curve is employed (black lines), as there is no evidence of hysteresis between the rising (filled circles) and falling (open circles) limbs of the hydrograph (see Methods). At Luang Prabang, there is likewise no evidence of hysteresis between the rising (coloured closed symbols) and falling (coloured open symbols) limbs. However, two rating functions are employed at this station, one for the pre-dam (orange coloured lines) and post-dam (green coloured lines) periods (see Methods).

Extended Data Figure 3. Daily flow discharge and suspended solids load at selected Mekong River gauging stations during 1st January 1995 to 31st December 1999. The left hand panels show daily simulated (Q_{sim}) and observed (Q_{obs}) water flows, along with the daily water flows attributable to tropical cyclones (Q_{sim_TC}) at **a**, Luang Prabang; **c**, Mukdahan; **e**, Pakse, and **g**, Stung Treng. The right hand panels show the daily total suspended solids load (Q_s; in megatonnes per day) and daily suspended solids load attributable to tropical cyclones (Q_{s_TC}; also in megatonnes per day) at **b**, Luang Prabang; **d**, Mukdahan; **f**, Pakse, and **h**, Stung Treng. Note that the period 1995 to 1999 encompasses the years during the 1981-2005 study period that are the most (1996) and least (1999) strongly affected by tropical cyclones.

Extended Data Table 2. Goodness of fit measures comparing VMod simulated and observed water flows at five river gauging stations on the Lower Mekong River. Note that the goodness of fit metrics are all based on the mean daily flows for the full simulation period (1st May 1981 to 31st March 2005), with the exception of the Mean Discrepancy Ratio for the annual flood peaks (Me_p). The Me_p metric is computed using the ratio of simulated maximum daily discharge to observed maximum daily discharge in each year of the record (1981-2004 inclusive) studied herein.

Extended Data Table 3. Mean annual hydrometeorological parameters (1982-2004) estimated at five hydrological stations on the Lower Mekong River. Errors represent one standard deviation around the mean annual loads. The Accumulated Cyclone Energy (ACE) for each station during the same period is also indicated.

Extended Data Figure 4. Time series of annual suspended solids load at selected river gauging stations during 1982 to 2004. **a,** Luang Prabang; **b,** Mukdahan; **c,** Pakse; **d,** Stung Treng. The symbols indicate the total suspended solids load (Q_s; open circles) and suspended solids load attributable to tropical cyclones (Q_{s_TC}; filled squares). Significant ($p \leq 0.05$) trends as identified by Mann-Kendall analysis are indicated by the dashed lines, with the corresponding time-rate of change of annual suspended solids load annotated on the plot.

Extended Data Figure 5. Spatial distributions of mean annual rainfall contributed from tropical cyclones over the Mekong Basin. **a**, 1981-1985; **b**, 1986-1990; **c**, 1991-1995; **d**, 1996-2000; **e**, 2001-2005. Note the pronounced declines in rainfall associated with tropical cyclones at Stung Treng and Kratie in particular.

Extended Data Figure 6. Strike counts for tropical cyclones tracking across the Mekong basin during 1950-2013. The strike count data plotted are extracted from the IBTrACS[41] database and normalized by the maximum count (199) observed in 1964. We employ strike count, rather than precipitation, data in this longer term historical analysis because reliable precipitation data are not available outside of the 1981-2005 period that is the main focus of the study. Similarly, mean wind speed data, which in principle could be used to estimate variations in Accumulated Cyclone Energy (ACE) as a proxy for precipitation, are available only sporadically outside of 1981-2005. In terms of strike counts, the data suggest there is a periodicity in the long term cyclone climatology, with the most recent data (2006-2013) having annual strike counts similar to the 1950-2013 mean of 87 ± 37. However, these data must be treated with caution since strike count data do not report the intensity or locations of cyclone tracks, both of which are important controls on the precipitation delivered to the basin by these TCs.

Extended Data Table 4. Suspended solids concentration (SSC) data sources used in constructing the sediment rating curves employed in this study. Number of samples refers to the total number of SSC data points used in the derivation of the sediment rating curves, with the numbers in parentheses indicating the number of SSC data points associated with tropical-cyclone induced runoff events. The latter are defined herein as runoff events for which at least 25% of the runoff was associated with tropical cyclone induced runoff. Consequently, it is only possible to identify tropical cyclone affected SSC measurements in the 1981-2005 model simulation period. Note that no tropical-cyclone induced runoff events were associated with the 60 SSC measurements made at Pakse during 1998-2002 and that the available data from Stung Treng and Kratie post-date the 1981-2005 study period.

Extended Data Figure 7. Procedures used to determine cross-section mean suspended sediment concentration from acoustic Doppler current profiler (aDcp) data. **a**, Calibration function (solid line; n = 54, r^2 = 0.9306, p < 0.0001) linking the suspended solids concentration (SSC) to acoustic backscatter (ABS) for the 600 kHz (RD Instruments) aDcp instrument employed in this study (dashed lines indicate 95% prediction intervals). **b**, Example of quasi-synoptic ABS field obtained from the aDcp survey at the Kratie gauging station on 23/09/2013 (flow discharge, Q = 57,000 m^3 s^{-1}). Note that there is a small blanking distance close to the water surface and a zone of side-lobe interference near the bed (indicated by the dashed black lines) where no ABS values are returned, and the ABS values in these zones are therefore determined by interpolation. **c**, Suspended solids concentration field obtained based on the ABS values in **b** and using the calibration function in **a**. Note how the locations of the nine point-based SSC estimates collected using the sampling procedure adopted at Luang Prabang and Pakse lead to a deviation of the cross-section mean SSC derived from the aDcp-estimated SSC field in **c** and the point-based sampling procedure. We compared 11 cross-section mean SSCs obtained using point-based versus aDcp sampling procedures at locations throughout the Mekong River south of Kratie to correct (by 26%) the consequent bias arising from cross-section averaging of point-based samples.